[2] Lamb, A. B., Bray, W. C., and Frazer, J. C. W., "The Removal of Carbon Monoxide from Air," *Journal of Industrial Engineering Chemistry*, Vol. 12, 1960, pp. 213–221.

[3] Brown, E. W., "Medical and Hygienic Aspects of the Submarine Service," *U.S. Navy Medical Bulletin*, Vol. 14, 1920, pp. 8–17.

[4] Carpenter, D. M., "Habitability of Submarines," *U.S. Navy, Medical Bulletin*, Vol. 26, 1928, pp. 31–40.

[5] Du Bois, E. F., "Review of Recent Work on Air Purification in Submarines," *Submarine Ventilation Bulletin No. 4*, March 1919, Bureau of Medicine and Surgery, Navy Dept.

[6] Miller, R. R. and Piatt, V. R., ed., "The Present Status of Chemical Research in Atmosphere Purification and Control on Nuclear-Powered Submarines," NRL Rept. 5465, April 1960, Naval Research Lab.

[7] Miller, R. R., "Alkali Metal Peroxy Compounds in Submarine Air Purification," NRL Rept. 5465, April 1960, Naval Research Lab.

[8] "Atmospheric Regeneration Aboard Submarines," Ionics Inc., Cambridge, Mass. Contract NObs-77048.

NOV.-DEC. 1968 J. AIRCRAFT VOL. 5, NO. 6

# A Vortex Method for the Study of Airplane-Missile Aerodynamic Interference

H. T. YANG*
*Hughes Aircraft Company, Canoga Park, Calif.*

**Within the slender body theory, a vortex method is developed for the study of aerodynamic interference between a missile, in both captive and dropped positions, and the carrying airplane. In the crossflow plane, the airplane fuselage is approximated by a circle represented by a doublet; the airplane wing, pylons, and the missile wing panels are represented by evenly distributed vortices. The case of a cruciform missile carried underneath a vertical pylon or dropped therefrom on each side of the airplane is considered. The normal force, side force, and rolling moment on the missile are computed for a typical geometry. They agree with results obtained by electric analogy performed on conducting papers with cutouts identical to the present model. Ways of improving the present method in the light of results obtained by electric analogy, wind tunnel, and flight test of actual configurations are indicated.**

## Nomenclature

$a$ = radius of airplane fuselage, ft
$b$ = radius of missile fuselage at the base, ft
$C_y$ = side force coefficient, $Y/(qS)$
$C_z$ = normal force coefficient, $Z/(qS)$
$C_l$ = rolling moment coefficient, $l/(qS\ 2b)$
$d$ = airplane wing elevation, ft
$e$ = horizontal pylon location from $z$ axis, ft
$f$ = location of lower edge of pylon from $y$ axis, ft
$g$ = horizontal missile location from $z$ axis, ft
$h$ = vertical missile location from $y$ axis, ft
$l$ = rolling moment, lb-ft
$L$ = length of missile, ft
$N$ = number of vortices representing the airplane wing panel
$P$ = number of vortices representing the pylon
$q$ = dynamic pressure, $\frac{1}{2}\rho_\infty U^2$, psf
$Q$ = number of vortices representing each missile wing panel
$S$ = cross-sectional area of the missile at the base, ft$^2$
$s$ = semispan of airplane wing, ft
$t$ = semispan of missile wing, ft
$U$ = forward velocity of missile, fps
$v$ = velocity component along $y$ axis, fps
$w$ = velocity component along $z$ axis, fps
$X$ = complex cross-flow plane, $y + iz$
$Y$ = side force, lb
$Z$ = normal force, lb
$\alpha$ = angle of attack, rad
$\Gamma$ = strength of circulation, ft$^2$ per sec
$\gamma$ = strength of vortex, ft$^2$ per sec
$\rho_\infty$ = mass density of freestream, slug/ft$^3$

***Subscripts***

0 = uniform crossflow
1 = airplane fuselage
2 = airplane wing
3 = airplane pylon
4 = first quadrant wing panel of the missile on the right
5 = second quadrant
6 = third quadrant
7 = fourth quadrant

Received February 27, 1967; revision received March 14, 1968. The author wishes to thank L. Wong, Manager of the Aerothermodynamics Department, for suggesting this problem and to thank his staff for support, in particular, G. W. Gage, who supplied electric analogy, wind-tunnel, and flight test data, and C. J. Feltman, for his contribution.

* Senior Staff Engineer, also Associate Professor of Aero-Space Engineering, University of Southern California, Los Angeles, Calif. Associate Fellow AIAA.

## Introduction

THE steady, irrotational flow over slender configurations at small angles of attack and of side slip may be treated by the slender body theory.[1–5] In essence, one deals with the Laplace equation in the crossflow plane subject to the boundary conditions on the body and far away from it. The validity of the theory is established by comparing results so obtained with more exact theory and experiments. The method of conformal mapping may be conveniently applied to simple shapes, such as plane- and cruciform-wing and body combinations. For complicated geometries, however, one does not always find the desired conformal transformations and must, therefore, resort to more approximate methods. One of these is the vortex method, treated independently by Nielsen[5] and by Campbell.[6,7] It was found[8] that Campbell's method is better suited for digital machine computation.

In Campbell's vortex method[6] for wing-body interference, the circular body is represented by a doublet in the uniform crossflow, and the thin wing panels by a finite number of evenly distributed discrete vortices. To maintain the shape of the circle as well as the constancy of flow circulation, one applies the method of images.[9] For each vortex introduced,

the image system consists of a vortex of opposite strength at the inverse point and a vortex of like strength at the center of the circle. If the flow circulation was originally zero, then the vortices at the center would cancel out. The no-flow conditions across the wing at an equal number of control points midway between two neighboring vortices determine the strengths of the distributed vortices, from which the loading is obtained. As a rule, the crossflow plane studied is at the maximum span station. The normal force, side force, and rolling moment on a pointed wing-body combination may be obtained from the loading in the maximum span crossflow plane. Campbell showed[6] that, for simple plane-wing and body combination, the vortex method converges from above to the solution obtained by conformal mapping, as the number of vortices increases.

The problem at hand is to find the aerodynamic loading, forces, and moments of a missile, captive or dropped within the interference field of the carrying airplane. The present work extends Campbell's vortex method for wing-body interference to the study of airplane-missile interference. In the crossflow plane, the airplane fuselage is approximated by a circle represented by a doublet; the airplane wing, pylons, and the missile wing panels are represented by evenly distributed vortices. To facilitate the application of image method, the missile fuselage is replaced by its wings. This is the lift carry-over assumption.[5] Its effect will later be discussed. The case of a cruciform missile carried underneath a vertical pylon or dropped therefrom on each side of the airplane is studied in detail. Computation is carried out in the crossflow plane corresponding to the maximum span station of the missile. From the strengths of the vortices, the aerodynamic loading on each of the wing panels is obtained. For a pointed missile, its normal force, side force, and rolling moment may be evaluated from the loading in this particular crossflow plane. These results agree with those from electric analogy performed on conducting papers with cutout exactly as the mathematical model, namely, circular airplane fuselage, infinitesimally thin wings and pylons, and vanishing missile fuselage. Comparisons are also made with electric analogy, wind tunnel, and flight tests conducted on practical configurations, which form the basis of improving the present method.

The determination of pitching moment and yawing moment on the missile involves a series of computations like the present one in a number of crossflow planes and then a numerical integration along the missile axis. This tedious computation has not been carried out. However, in view of the wind-tunnel and flight test results mentioned in the next section, no anomalous behavior is to be expected.

## Assumptions

The basic assumptions introduced in the present work are the following:

1) Slender body theory. The validity of slender body theory is well established for slender wings, bodies, and wing-body combinations. The theory shows the force and moment coefficients do not depend on the Mach number and they vary linearly with angles of attack. In connection with the present airplane-missile interference problem, wind-tunnel tests were conducted at the LTV 4-ft high-speed wind tunnel, at Mach numbers 0.7, 0.9, 0.95, 1.05, 1.2, and 1.58. In addition flight tests were conducted in Southern California at Mach numbers 0.4, 0.7, 0.8, 0.9, 1.1, 1.2, and 1.6. The data on normal force, side force, rolling moment, and pitching moment do show a linear dependence on angles of attack between $-2°$ and $10°$. The slopes of these curves show little dependence on Mach numbers. In other words, interfering shock waves, if any, do not show any net effect on the gross forces and moments, in the present range of Mach numbers and angles of attack.

2) Neglect of flow separation. At moderately high angles of attack, flow separates from slender wings, bodies, and wing-body combinations. The normal force, for example, is larger than that predicted by attached crossflow analysis. The difference is attributed to nonlinear effects. In the tests mentioned in the preceding paragraph, the resultant nonlinear effects simply do not show up in the airplane-missile interference problem. In addition, a tuffed captive missile was flown during the flight test. No appreciable flow separation was observed. The neglect of flow separation is therefore justified in the present analysis.

3) Replacement of missile body by wings. Aerodynamically, this simplification amounts to the missile body providing full lift carry-over.[5] The error involved in such an approximation may be estimated by formulas developed for a free missile consisting of triangular cruciform wings on a pointed body. From Eq. (5-35) of Ref. 5, the ratio of lift coefficient for the wing-body combination to that for the wing alone is, in our present notation,

$$C_z/C_{z_w} = 1 - (b/t)^2 + (b/t)^4 \qquad (1)$$
$$(1/\alpha)C_{z_w} = 2(t/b)^2$$

based on the cross-sectional area of the missile fuselage $S = \pi b^2$. This ratio has a minimum value of $\frac{3}{4}$ at $b/t = (\frac{1}{2})^{1/2}$. In other words, the maximum error in assuming lift carry-over is an overestimation of lift by 33%. For the missile geometry considered in this paper, $b/t = 0.409$, the error is only half that much, namely, 16%. It is conceivable that, in the present analysis of airplane-missile interference, the error introduced by assuming lift carry-over on the missile would be of the same order of magnitude. A method is suggested toward the end of the paper to remove this simplification, together with other recommendations.

## Flow Configuration and Complex Velocities

The airplane, together with its missiles in the crossflow plane, is depicted in Fig. 1. The plane is designated

$$X = y + iz \qquad (2)$$

There are five aerodynamic components, whose complex velocities will be written down in the notation of Glauert.[10]

0) Uniform crossflow $U\alpha$. $U$ is the forward velocity of the missile whose angle of attack $\alpha$ is small. The complex velocity is

$$v_0 - iw_0 = -iU\alpha \qquad (3)$$

where $v$ and $w$ are the velocity components along $y$ and $z$ axis, respectively.

1) The airplane fuselage approximated by a circular cylinder of radius $a$ is represented by a doublet situated at the origin whose complex velocity is

$$v_1 - iw_1 = -iU\alpha a^2/X^2 \qquad (4)$$

2) The airplane wing with elevation $d$ and semispan $s$ is represented by $N$ evenly distributed vortices on either exposed wing span. The location of $j_2$th vortex of strength $\gamma_{j_2}$ is

$$X_{j_2} = (a^2 - d^2)^{1/2} + j_2[s - (a^2 - d^2)^{1/2}]/N + id \qquad (5)$$
$$j_2 = 1, \ldots, N$$

The boundary condition on the circular fuselage is satisfied by the method of images that consist of a vortex of strength $-\gamma_j$ at the inverse point

$$a^2/\bar{X}_{j_2} \equiv a^2 X_{j_2}/|X_{j_2}|^2$$

and a vortex of strength $\gamma_{j_2}$ at the center of the circular cylinder.[9] The complex velocity due to the wing vortices on

the left and right and the images inside the fuselage is

$$v_2 - iw_2 = -\frac{i}{2\pi}\sum_{j_2=1}^{N}\gamma_{j_2}\left[\frac{1}{(X - X_{j_2})} - \frac{1}{(X + \bar{X}_{j_2})} - \frac{1}{(X - a^2X_{j_2}/|X_{j_2}|^2)} + \frac{1}{(X + a^2\bar{X}_{j_2}/|X_{j_2}|^2)}\right] \quad (6)$$

where $\gamma_{j_2}$ is positive, counterclockwise. Note that the image vortices at the origin cancel each other due to symmetry.

3) Similarly, the pylon at a horizontal distance $e$ from the $z$ axis with a length $d - f$ is represented by $P$ vortices at

$$X_{j_3} = e + i[d + j_3(f - d)/P]$$
$$j_3 = 1,\ldots,P \quad (7)$$

The complex velocity due to pylon vortices and their images takes the same form as Eq. (6), with the replacement of subscript 2 by subscript 3, and $N$ by $P$.

4) The missile cruciform wing with semispan $t$ is represented by $Q$ vortices on each of the four panels. The location of $j_4$th vortex on the first quadrant wing panel on the right is

$$X_{j_4} = g + j_4t/(2^{1/2}Q) + i[h + j_4t/(2^{1/2}Q)]$$
$$j_4 = 1,\ldots,Q \quad (8)$$

The complex velocity due to the vortices on the first quadrant panel on the right and those on the second quadrant on the left take the same form as Eq. (6), with the replacement of subscript 2 by subscript 4, and $N$ by $Q$. The location of the $j_5$th vortex on the second quadrant panel on the right missile is $X_{j_5}$ given by Eq. (8), with subscript 4 replaced by subscript 5, and the plus sign of the second term by a minus sign. The corresponding complex velocity takes the same form as Eq. (6), with the replacement of subscript 2 by subscript 5, and $N$ by $Q$. For the third quadrant, we replace in Eq. (8) subscript 4 by subscript 6 and the plus signs of the second term and that inside the square bracket by minus signs, and in Eq. (6), subscript 2 by subscript 6, and $N$ by $Q$. Finally, for the fourth quadrant, replace in Eq. (8) subscript 4 by subscript 6 and the plus sign inside the square bracket by a minus sign, and in Eq. (6), subscript 2 by subscript 7, and $N$ by $Q$. The resultant induced complex velocity at $X \equiv y + iz$ due to all the distributed vortices and their images inside the circular cylinder is

$$v - iw = (v_2 + v_3 + v_4 + v_5 + v_6 + v_7) - i(w_2 + w_3 + w_4 + w_5 + w_6 + w_7) \quad (9)$$

5) The missile fuselage of radius $b$ situated at $(g, h)$. For captive missiles, $g = e$, $h = f$. As discussed in assumption 3, the missile fuselage will be replaced by its cruciform wings.

## Boundary Conditions

The velocity potentials, from which the preceding velocity components are derived for the uniform crossflow, doublet, and vortices, satisfy the Laplace's equation in the crossflow plane. By superposition, any linear combination of the velocity potentials also satisfies the governing Laplace's equation. It remains to satisfy the boundary conditions through which the unknown strengths $\gamma$'s of the distributed vortices are determined. The arbitrariness of the solution is thus removed.

0) At infinity $|X| \to \infty$. As can be seen from Eqs. (4) and (6), all the velocity components due to the doublet and vortices vanish at infinity. The crossflow there is uniform as given by Eq. (3).

1) On the fuselage, the boundary condition on the circularly cylindrical fuselage is satisfied by the method of images discussed following Eq. (5). The $N + P + 4Q$ unknown

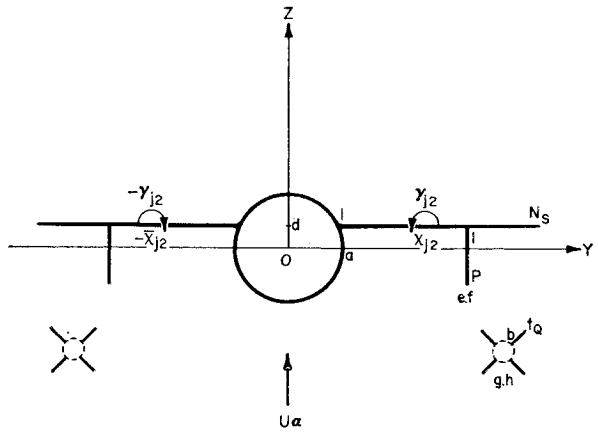


**Fig. 1 Airplane-missile configuration in the crossflow plane.**

vortex strengths are determined by the boundary conditions of no flow normal to the airplane wings, pylons, and the cruciform missile wings at $N + P + 4Q$ control points midway between two neighboring vortices.

2) On the wing, the control points are located at

$$X_{k_2} = (a^2 - d^2)^{1/2} + (k_2 - \tfrac{1}{2}) \times [s - (a^2 - d^2)^{1/2}]/N + id$$
$$k_2 = 1,\ldots,N \quad (10)$$

The no-flow boundary condition is

$$v_0 - iw_0 + v_1 - iw_1 + v - iw = 0$$

Using Eqs. (3) and (4), we have

$$w(X_{k_2}) = -U\alpha[1 + a^2Rl(1/X_{k_2}^2)]$$
$$k_2 = 1,\ldots,N \quad (11)$$

3) On the pylon, the control points are at

$$X_{k_3} = e + i[d + (k_3 - \tfrac{1}{2})(f - d)/P]$$
$$k_3 = 1,\ldots,P \quad (12)$$

The no-flow boundary condition across becomes

$$v(X_{k_3}) = U\alpha a^2Rl(i/X_{k_3}^2)$$
$$k_3 = 1,\ldots,P \quad (13)$$

4) On the cruciform missile wing, the control points for the first quadrant wing panels of the missile on the right are at

$$X_{k_4} = g + (k_4 - \tfrac{1}{2})t/(2^{1/2}Q) + i[h + (k_4 - \tfrac{1}{2})t/(2^{1/2}Q)] \quad (14)$$

The no-flow boundary conditions normal to the cruciform wing panel are

$$Im\{[(v_0 - iw_0) + (v_1 - iw_1) + (v - iw)]\exp[i(\pi/4)]\} = 0$$

With Eqs. (3) and (4), the preceding equation becomes

$$v(X_{k_4}) - w(X_{k_4}) = U\alpha[1 + a^2Rl(i/X_{k_4}^2) + a^2Im(i/X_{k_4}^2)]$$
$$k_4 = 1,\ldots,Q \quad (15)$$

The location of the control points in the second, third, and fourth quadrants are, respectively,

$$X_{\substack{k_5\\6\\7}} = g \mp (k_5 - \tfrac{1}{2})t/(2^{1/2}Q) + i[h \pm (k_5 - \tfrac{1}{2})t/(2^{1/2}Q)]$$
$$k_5 = 1,\ldots,Q \qquad k_6 = 1,\ldots,Q \qquad k_7 = 1,\ldots,Q \quad (16)$$

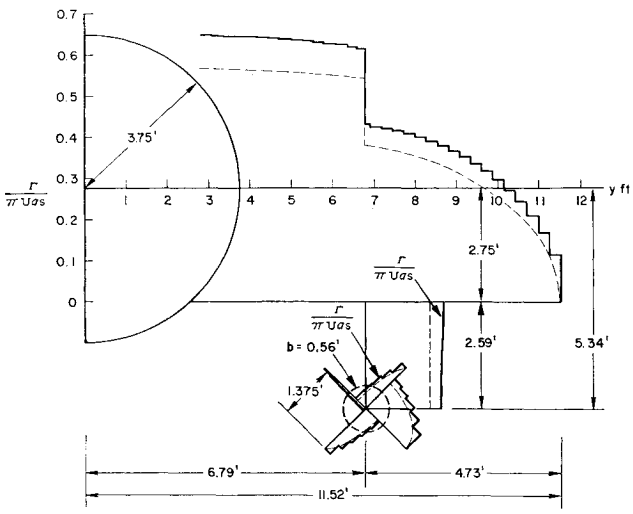


**Fig. 2 Load distribution on airplane and captive missile.**

The corresponding boundary conditions are, respectively,

$$v(X_{k_5}) \mp w(X_{k_5}) = U\alpha[\mp 1 + a^2Rl(i/X_{k_5}^2) \mp a^2Im(i/X_{k_5}^2)] \quad (17)$$

Equations (11, 13, 15, and 17) constitute $N + P + 4Q$ simultaneous linear algebraic equations to be solved for $N + P + 4Q$ unknown vortex strengths $\gamma$'s. In other words, the solution of the linear partial differential equation of Laplace with complicated boundaries reduces to the solution of a system of linear algebraic equations. In the case of wing-body combination, it is shown that[6] the present scheme approaches the known exact solution[1,5] from above when the number of vortices on the wing, $N$, increases without limit. Conceivably, in the present computation, the accuracy of the results will be improved by increasing $N$, $P$, and $Q$. Since there are three integers $N$, $P$, and $Q$ in the present airplane-missile interference instead of one integer $N$ in the wing-body interference, care must be exercised in increasing $N$, $P$, and $Q$. It is recommended that the integers $N$, $P$, and $Q$ be in proportion to the airplane exposed semispan, pylon height, and the missile cruciform wing semispan. Symbolically

$$N:P:Q \approx [s - (a^2 - d^2)^{1/2}]:(d - f):t \quad (18)$$

In this way, we shrink uniformly the cell size in the $NPQ$ space by increasing $N$, $P$, and $Q$ proportionally.

Once the strengths of the vortices are known, the loading, forces, and moments may readily be evaluated. Of particular interest are these quantities on the missile, for which detailed expressions will be given in the next section.

## Aerodynamic Loading, Normal Force, Side Force, and Rolling Moment on the Missile

The load distribution for the first quadrant wing panel of the missile on the right is

$$\Gamma_{j_4} = \sum_{n_4=j_4}^{Q} \gamma_{n_4} \qquad 1 \le j_4 \le Q \quad (19)$$

To calculate total forces for a pointed slender body, one only needs the crossflow at the maximum span station which in the present case is the base.[5] Applying the theorem of Kutta and Joukowski, we get the normal force and side force on the panel,[6,7]

$$Z_4 = \rho_\infty U \sum_{j_4=1}^{Q} \Gamma_{j_4} |Rl(X_{j_4} - X_{j_4-1})| \quad (20)$$

$$Y_4 = -\rho_\infty U \sum_{j_4=1}^{Q} \Gamma_{j_4} |Im(X_{j_4} - X_{j_4-1})| \quad (21)$$

where

$$X_{j_4-1=0} = g + ih \quad (22)$$

This theorem is valid in the linearized theory of two-dimensional subsonic and supersonic flows, where the pressure coefficient is equal to $-2$ times the perturbation velocity in the freestream direction, divided by the freestream velocity. The lift, which is a result of pressure difference between the lower and upper surfaces of the airfoil, will then be equal to the product of freestream density and velocity, and the circulation around the airfoil. The rolling moment exerted by this panel about the axis is

$$l_4 = \rho_\infty U \sum_{j_4=1}^{Q} \Gamma_{j_4} |X_{j_4} - X_{j_4-1}|(\tfrac{1}{2}|X_{j_4} - X_{j_4-1}| + |X_{j_4-1} - X_0|) \quad (23)$$

The corresponding quantities in the second, third, and fourth quadrant are, respectively,

$$\Gamma_{\substack{j_5 \\ 6 \\ 7}} = \sum_{\substack{j_5=1 \\ 6 \\ 7}}^{Q} \gamma_{n_5} \qquad 1 \le \underset{6}{j_5} \le Q \quad (24)$$

$$Z_{\substack{5 \\ 6 \\ 7}} = \mp \rho_\infty U \sum_{j_5=1}^{Q} \Gamma_{\substack{j_5 \\ 6 \\ 7}} |Rl\,(X_{\substack{j_5 \\ 6 \\ 7}} - X_{\substack{j_5-1 \\ 6 \\ 7}})| \quad (25)$$

$$Y_{\substack{5 \\ 6 \\ 7}} = \mp \rho_\infty U \sum_{j_5=1}^{Q} \Gamma_{\substack{j_5 \\ 6 \\ 7}} |Im(X_{\substack{j_5 \\ 6 \\ 7}} - X_{\substack{j_5-1 \\ 6 \\ 7}})| \quad (26)$$

$$l_{\substack{5 \\ 6 \\ 7}} = \rho_\infty U \sum_{j_5=1}^{Q} \Gamma_{\substack{j_5 \\ 6 \\ 7}} |X_{\substack{j_5 \\ 6 \\ 7}} - X_{\substack{j_5-1 \\ 6 \\ 7}}| \times (\tfrac{1}{2}|X_{\substack{j_5 \\ 6 \\ 7}} - X_{\substack{j_5-1 \\ 6 \\ 7}}| + |X_{\substack{j_5 \\ 6 \\ 7}} - X_0|) \quad (27)$$

The resultant normal force, side force, and rolling moment about the axis of the missile on the right are

$$\begin{aligned} Z &= Z_4 + Z_5 + Z_6 + Z_7 \\ Y &= Y_4 + Y_5 + Y_6 + Y_7 \\ l &= l_4 + l_5 + l_6 + l_7 \end{aligned} \quad (28)$$

The sign convention is that the forces are positive along the positive axis directions and the rolling moment is positive, top inboard. In terms of coefficients, one has

$$\begin{aligned} C_Z/\alpha &= Z/(\alpha qS) \\ C_Y/\alpha &= Y/(\alpha qS) \\ C_l/\alpha &= l/(\alpha qS2b) \end{aligned} \quad (29)$$

The foregoing equations have been programmed for an electronic digital computer IBM 7094.

To obtain the pitching moment $m$ and yawing moment $n$, we make use of Eq. (3-65) of Ref. 5,

$$m - in = iL[Y(L) + iZ(L)] - i\int_0^L [Y(X) + iZ(X)]dX \quad (30)$$

Here $L$ is the length of the missile. $Y(L)$ and $Z(L)$ are the normal force and side force acting on the missile which have already been found. To evaluate the second term, one has to find the normal force $Y(X)$ and side force $Z(X)$ in a number of crossflow planes and perform a numerical integration along the missile axis. The laborious computation in a series of

**Table 1 Force and moment coefficients dependence on number of vortices**

| $N$ | $P$ | $Q$ | $(1/\alpha)C_z$ | $(1/\alpha)C_y$ | $(1/\alpha)C_l$ |
|---|---|---|---|---|---|
| 1 | 1 | 1 | 3.53 | 6.37 | 6.17 |
| 7 | 2 | 1 | 6.30 | 7.75 | 11.45 |
| 13 | 4 | 2 | 5.33 | 6.72 | 9.24 |
| 20 | 6 | 3 | 5.02 | 6.38 | 8.40 |
| 26 | 8 | 4 | 4.86 | 6.19 | 8.07 |
| 33 | 9 | 5 | 4.77 | 6.08 | 7.86 |

crossflow planes like the present one has not been carried out. In view of the wind-tunnel and flight test data mentioned previously, a linear dependence of the pitching and yawing moment coefficients on the angle of attack is to be expected.

## Illustrative Example

A typical case of airplane-missile interference is computed for the following data: $s = 11.52$, $a = 3.75$, $b = 0.5625$, $d = -2.75$, $g = e = 6.79$, $f = -5.339$, $t = 1.375$, all in feet; $U = 1{,}039$ fps, $q = 700$ psf. The cases of missile in captive and dropped positions and by itself were worked out.

For the missile in captive, $h = f = -5.339$ ft. We first computed by hand the approximation $N = 1$, $P = 1$, and $Q = 1$, resulting in six simultaneous equations, which checked out the machine computation. According to Eq. (18), the recommended ratio is $N:P:Q = 6.52:1.88:1$. The computed results, improving as the number of vortices increases, are summarized in Table 1.

As can be seen, the results converge from above as the number of vortices increases. Hereafter, we shall use $Q = 5$, which yields results within 3% of $Q = 4$. The detailed load distribution on the cruciform missile wing panels as well as that on the airplane wing and pylon is shown in Fig. 2, for $Q = 5$. The loading on the missile is not symmetric due to interference with the airplane. When the missile is by itself, the loading is symmetric as shown in Fig. 3. The load on the missile is transmitted to the pylon, by adding the strengths of missile vortices to those of the pylon vortices. Basically, the missile vortex and its image in the airplane fuselage form a bound vortex by going through the pylon and the airplane wing. By this very mechanism, the loading on the missile and that on the pylon are transmitted to the airplane wing. As a result, there is a jump in the airplane wing loading across the pylon location.

**Table 2 Comparison of vortex method with other methods**

| | $(1/\alpha)C_Z$ | $(1/\alpha)C_Y$ | $(1/\alpha)C_l$ |
|---|---|---|---|
| | | Captive | |
| Vortex method 1 | 4.77 | 6.08 | 7.86 |
| Electric analogy 1 | 4.37 | 6.09 | 7.42 |
| Electric analogy 2 | 5.71 | 15.3 | 7.7 |
| Wind tunnel 2 | 6.7 | 14.8 | 6.1 |
| Flight test 2 | 6.6 | 11 | 4.1 |
| | | 1.25-ft drop | |
| Vortex method 1 | 6.316 | 9.21 | 1.974 |
| Electric analogy 1 | 6.321 | 9.71 | 0.309 |
| Electric analogy 2 | 6.6 | 9.9 | 0.268 |
| | | Missile by itself | |
| Vortex method[a] 1 | 13.21 | 0.00000 | 0.00019 |
| Electric analogy 1 | 12.72 | 0 | 0 |
| Slender body theory 1 | 11.95 | 0 | 0 |
| Electric analogy 2 | 10.31 | 0 | 0 |
| Slender body theory 2 | 10.29 | 0 | 0 |
| Wind tunnel 2 | 10.9 | 0 | 0 |

[a] Simulated by a vertical drop of $10^4$ ft.

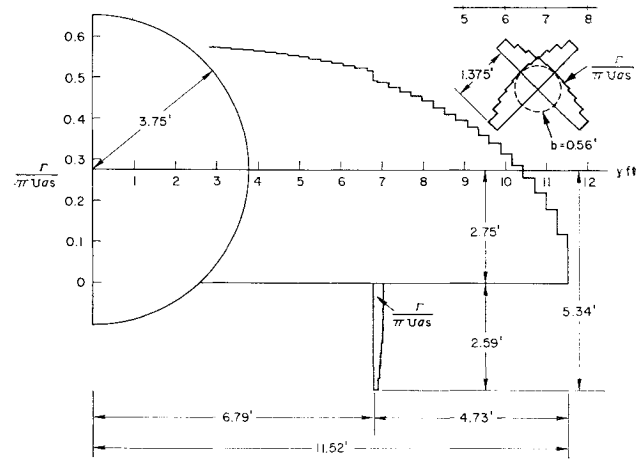


**Fig. 3 Load distribution on airplane and missile dropped vertically $10^4$ ft.**

One of the dropped positions studied is at 1.25 ft. Here $h = -6.589$ ft. The load distribution is shown in Fig. 4. Due to interference with the airplane, the missile loading is again unsymmetric. This load is not transmitted to the pylon because they are not connected. The pylon load is appreciable due to interference and is transmitted to the airplane wing to cause a jump in loading. Note that the circulation around the missile is $0.036\ U\alpha s$, rather than zero as it should be. If the missile fuselage were not neglected, as in assumption 3, the image vortices inside it would cancel all the vortices distributed along the wing panels. Summarized in Table 2 are the force and moment coefficients.

The missile alone case is simulated by a vertical drop of $10^4$ ft; thus $h = -10{,}005.339$ ft. The load distribution is shown in Fig. 3, and it is approximately elliptic on all components. The circulation around the missile is $3 \times 10^{-6}\ U\alpha s$, practically zero. Note that the loading on the vertical pylon is very small. The force and moment coefficients are summarized in Table 2. As a check, the loading on the wing and the pylon agree with the captive case when the number of vortices on each missile panel is set equal to zero, i.e., $Q = 0$.

The loading on the airplane wing and pylon and on the missile panels agrees with those of electric analogy results of case 1 (identical geometry), which are plotted as dashed lines in Fig. 2.

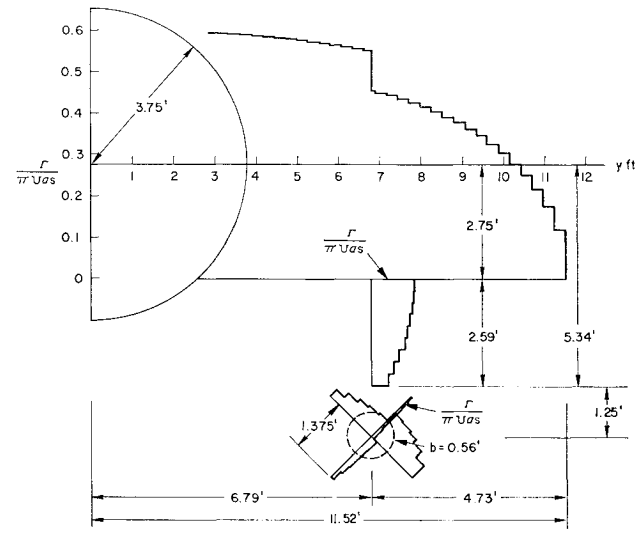


**Fig. 4 Load distribution on airplane and missile dropped vertically 1.25 ft.**

## Comparison with Other Methods

The airplane-missile interference problem has been studied not only by the present vortex method, but also by the methods of electric analogy, wind tunnel, and flight test. The comparison of these methods is summarized in Table 2. The numeral 1 after the method designates the simple mathematical model of Fig. 1 with dimensions given in the last section. Numeral 2 refers to scale cutout in electric analogy, scale model in wind tunnel of the full-size actual vehicles in the flight test.

From Table 2, the following observations may be made:

1) Captive missile. The comparison between the present vortex method and electric analogy 1 is very satisfactory. It is to be expected, because both methods solve Laplace's equation for the same boundary conditions. Electric analogy 2 and wind tunnel 2 agree fairly well, which once more justifies the assumptions 1 and 2. The side forces are higher by both methods. It is to be remembered that the edge effect of the conducting paper and the wind-tunnel wall effect are present. In electric analogy 1, the correction for edge effects can be readily made because of its simple geometry. The scatter of the flight test 2 data is about 10%. For captive flight, the vortex method yields the lower limit of the normal force and the side force and the upper limit of the rolling moment. Here the vortex method should be used together with the electric analogy method 2. Of course wind-tunnel and particularly flight tests are desirable, but they are very expensive to run.

2) Trajectory position. It is interesting to note here that the detailed geometry does not matter much in the electric analogy. This is because the missile is away from the airplane, whose fuselage may be approximated by an equivalent circle, so far as the net effect on the missile is concerned. The vortex method, therefore, agrees with the electric analogy except for the rolling moment. This is due to the nonvanishing circulation around the missile mentioned in the last section. It is difficult to obtain the normal force, side force, and rolling moment coefficients slopes from wind-tunnel data at this position. The flight test data for such positions have not been attempted. The utility of the vortex method as well as of electric analogy lies here. Between the two, the vortex method yields results very readily once it is programmed. The electric analogy requires repetitious measurements for each configuration.

3) Free missile. Here the different methods yield essentially the same result. In other words, the wing-body interference of a missile within the slender body theory causes no particular problem. The airplane-missile interference still warrants much study. It is gratifying to note that the vortex method recovers the free missile as a limiting case. We also note the slender body theory results are obtainable from Eq. (1). For the present geometry, $b/t = 0.409$

$$C_z/C_{zw} = 0.8607$$

$$(1/\alpha)C_{zw} = 11.95$$

$$(1/\alpha)C_z = 10.29$$

The $Q = 5$ approximation in the vortex method overestimates $C_{zw}$ by 10% and gives practically zero side force and rolling moment as it should.

## Conclusion and Discussion

A vortex method is developed, within the linear slender body theory, for the missile in captive or dropped positions in the interference field of the airplane. The aerodynamic loading, normal force, side force, and rolling moment on the missile are computed in detail for a typical geometry. The results so obtained are compared with those from electric analogy, wind tunnel, and flight test. For the missile in captive position, the present method serves as an aid in the analysis of complicated installations. For the missile in trajectory position, the present method is a useful tool by itself, except it overestimates the rolling moment somewhat. Finally, the vortex method recovers the results for free missile as a limiting case.

The vortex method in the present form is an initial step in the analysis of the complicated problem of airplane-missile interference. Improvement can certainly be made in the following directions:

1) The effect of compressibility and nonslender body. In reducing the three-dimensional perturbation potential equation to the two-dimensional Laplace's equation, the assumption is made that

$$|M_\infty^2 - 1|[(2t)^2/L^2] \ll 1$$

where $M_\infty$ is the freestream Mach number and $2t/L$ is the fineness ratio of the body. The accuracy of the theory may be improved by expanding the velocity potential in powers of the ratio

$$|M_\infty^2 - 1|[(2t)^2/L^2]$$

This has been done for simple shapes in Refs. 4, 11, and 12. The same correction may be made here. However, in view of the test results mentioned, this effect may be ignored.

2) The nonlinear effect of separated flow. This nonlinear effect is very important for wings, bodies, and wing-body combinations such as missiles. Various methods of analysis have been developed. See, for instance, Ref. 13. Again as shown in the test results, the nonlinear effect in the airplane-missile interference problem is not as important. This is so for the present configuration at angles of attack between $-2°$ to $10°$ and Mach number up to 1.6, for which the present vortex method is intended.

3) The effect of the missile fuselage. The third assumption may be removed by applying the circle theorem of Milne-Thomson.[9] One finds the complex potential $f(X)$ for the flowfield outside the missile fuselage which is neglected first. Then introduce the circular missile fuselage of radius $b$. According to the circle theorem, the resultant complex potential is $f(X) + \bar{f}(b^2/X)$, from which the complex velocity may be found. The analysis then continues the same way as in the preceding. The correction thus obtained may be a minor one, but it will yield better results for rolling moment.

4) The general shape of the airplane. With the restoration of the missile fuselage in the analysis, the missile is accurately described. The airplane fuselage is, in general, not exactly circular, and the wings and pylons have thicknesses. To study the general shape of the airplane, there are conformal transformations[14,15] available to transform it into a circle. These are numerical in nature and tedious to carry out. This correction will improve the results for the missile in the captive position, but not by much in the trajectory position.

5) Unsymmetric load. The unsymmetric loading condition may develop when one missile is in the trajectory position, while the other is in captive. The vortex method handles the unsymmetric load with ease. The present author has obtained the load distribution on unsymmetric wing body combinations by both the analytical method and the vortex method. The vortex result again converges to the exact solution from above. In the present configuration, special care must be taken of the nonvanishing image vortices at the center of the circle[8] approximating the airplane fuselage. The interference between the missile on one side or the airplane and the missile on the other side is not as important as the interference between the airplane and the missile. The reason is that the missiles are relatively small in size and far away from each other. In the flight test mentioned previously both symmetric and unsymmetric installations of the missile were flown, and no significant difference in missile loads were recorded. In fact, this confirms the philosophy in the wind-tunnel test with the missile model installed only on one side of the airplane model.

6) More complicated configurations. The present vortex method has been extended to more complicated configurations. One of them involves as many as four missile-launchers on a vertical pylon (two on each side of the pylon), and the other has two vertical pylon-missile combinations on each side of the airplane.

## References


[1] Spreiter, J. R., "The Aerodynamic Forces on Slender Plane- and Cruciform-Wing and Body Combinations," TR 962, 1950, NACA.

[2] Spreiter, J. R., "On Slender Wing-Body Theory," *Journal of the Aeronautical Sciences*, Vol. 19, No. 8, Aug. 1952, pp. 571–572.

[3] Ward, G. N., "Supersonic Flow past Slender Pointed Bodies," *Quarterly Journal of Mechanics and Applied Mathematics*, Vol. 2, Pt. 1, 1949, pp. 75–97.

[4] Adams, M. C. and Sears, W. R., "Slender-Body Theory–Review and Extension," *Journal of the Aeronautical Sciences*, Vol. 20, No. 2, Feb. 1953, pp. 85–98.

[5] Nielsen, J. N., *Missile Aerodynamics*, 1st ed., McGraw-Hill, New York, 1960, pp. 131–140, pp. 156–165.

[6] Campbell, G. S., "A Finite Vortex Method for Slender Wing-Body Combinations," *Journal of the Aeronautical Sciences*, Vol. 25, No. 1, Jan. 1958, pp. 60–61.

[7] Campbell, G. S., "Characteristics of Slender Wing-Body Combinations with Folding Wings," *Aircraft Engineering*, Jan. 1959, pp. 1–8.

[8] Yang, H. T., "Remarks on the Vortex Model of Wing-Body Interference," *AIAA Journal*, Vol. 5, No. 3, March 1967, p. 607.

[9] Milne-Thomson, L. M., *Theoretical Hydrodynamics*, 5th ed., Macmillan, New York, 1968, p. 157, p. 364.

[10] Glauert, H., *The Elements of Airfoil and Airscrew Theory*, 2nd ed., Cambridge University Press, New York, 1947, p. 55.

[11] Lawrence, H. R., "The Lift Distribution on Low Aspect Ratio Wings at Subsonic Speeds," *Journal of the Aeronautical Sciences*, Vol. 18, No. 10, Oct. 1951, p. 638–695.

[12] Lomax, H. and Sluder, L., "Chordwise and Compressibility Corrections to Slender Wing Theory," TR 1105, 1952, NACA.

[13] Sacks, A. H., Lundberg, R. E., and Hanson, C. W., "A Theoretical Investigation of the Aerodynamics of Slender Wing-Body Combinations Exhibiting Leading-Edge Separation," CR-719, March 1967, NASA.

[14] Sacks, A. H., "Aerodynamic Forces, Moments, and Stability Derivatives for Slender Bodies of General Cross Section," TN 3283, Nov. 1954, NACA.

[15] Skulsky, R. S., "A Conformal Mapping Method to Predict Low-Speed Aerodynamic Characteristics of Arbitrary Slender Re-Entry Shapes," *Journal of Spacecraft and Rockets*, Vol. 3, No. 2, Feb. 1966, pp. 247–253.


NOV.-DEC. 1968 J. AIRCRAFT VOL. 5, NO. 6

# Review of Methods for Predicting the Aerodynamic Characteristics of Parawings


MICHAEL R. MENDENHALL,* SELDEN B. SPANGLER,† AND JACK N. NIELSEN‡

*Nielsen Engineering & Research Inc., Palo Alto, Calif.*



**A review is made of methods for predicting the aerodynamic characteristics of one- and two-lobed conical parawings and all-flexible parawings, with emphasis on the low-speed characteristics of conical two-lobed parawings. Methods are reviewed and compared for predicting canopy shape and parawing lift, drag, and pitching moment. A discussion is given of the effects of leading-edge booms on the aerodynamic characteristics. Comparison is made between experiment and prediction for flexible parawings and rigid wings of parawing shape.**


## Nomenclature

$A$ = aspect ratio, $b^2/S$
$b$ = span of wing
$c$ = local chord
$c_d$ = section drag coefficient, based on local chord
$c_l$ = section lift coefficient, based on local chord
$c_{l\alpha}$ = section lift-curve slope, per rad
$c_{l_{max}}$ = maximum section lift coefficient
$c_r$ = root chord
$C_D$ = wing drag coefficient, based on planform area $S$
$C_{Di}$ = wing-induced drag coefficient, based on planform area $S$
$C_L$ = wing lift coefficient, based on planform area $S$
$C_{L\alpha}$ = wing lift-curve slope, $dC_L/d\alpha$, per rad
$C_m$ = wing pitching-moment coefficient, based on planform area $S$, and mean aerodynamic chord
$C_{m_\alpha}$ = wing moment-curve slope, $dC_m/d\alpha$, per rad
$C_{m_0}$ = wing pitching-moment coefficient at zero wing lift
$d$ = diameter of leading-edge boom
$f$ = maximum ordinate of camber section
$l$ = projected trailing-edge length of inflated parawing measured in planform
$l_0$ = value of $l$ for uninflated planform
$l'$ = canopy trailing-edge length of inflated triangular parawing
$q$ = freestream dynamic pressure
$s$ = semispan
$S$ = wing planform area, inflated
$T$ = spanwise tension per unit chord
$x, y, z$ = wing axes, Fig. 1
$\alpha$ = angle of attack
$\alpha_0$ = angle of attack for zero lift
$\alpha_l$ = luffing angle of attack
$\epsilon$ = semiapex angle of inflated planform
$\lambda$ = tension parameter, Eq. (1)
$\Lambda$ = sweep angle of leading edge of inflated planform
$\beta$ = half of angle subtended at cone axis by a parawing lobe lying on the surface of a circular cone; a half-cone corresponds to $\beta = 90°$
$\Delta\Lambda$ = difference in sweep angle of leading edge between inflated and uninflated states

***Subscripts***

$M$ = value given by Multhopp method
$W$ = value given by Weissinger method


Presented as Paper 68-10 at the AIAA 6th Aerospace Sciences Meeting, New York, January 22–24, 1968; submitted January 11, 1968; revision received June 20, 1968.



* Research Engineer. Associate Member AIAA.

† Vice President. Fellow AIAA.

‡ President. Associate Fellow AIAA.